Hyperglycemia Induces Bioenergetic Changes in Adipose-Derived Stromal Cells While Their Pericytic Function Is Retained

Hajmousa, Ghazaleh; Elorza, Alvaro A.; Nies, Vera J. M.; Jensen, Erik L.; Nagy, Ruxandra A.; Harmsen, Martin C.

Published in:
Stem cells and development

DOI:
10.1089/scd.2016.0025

Publication date:
2016

STEM CELLS AND DEVELOPMENT
Volume 25, Number 19, 2016

DOI: 10.1089/scd.2016.0025

Hyperglycemia Induces Bioenergetic Changes in Adipose-Derived Stromal Cells While Their Pericytic Function Is Retained

Ghazaleh Hajmousa,[1] Alvaro A. Elorza,[2,3] Vera J.M. Nies,[4] Erik L. Jensen,[3] Ruxandra A. Nagy,[1] and Martin C. Harmsen[1]

Diabetic retinopathy (DR) is a hyperglycemia (HG)-mediated microvascular complication. In DR, the loss of pericytes and subsequently endothelial cells leads to pathologic angiogenesis in retina. Adipose-derived stromal cells (ASC) are a promising source of therapeutic cells to replace lost pericytes in DR. To date, knowledge of the influence of HG on the bioenergetics and pericytic function of ASC is negligible. Human ASC were cultured in normoglycemia medium (5 mM D-glucose) or under HG (30 mM D-glucose) and assessed. Our data showed that HG increased the level of apoptosis and reactive oxygen species production in ASC, yet their proliferation rate was not affected. HG induced alterations in mitochondrial function and morphology in ASC. HG also strongly affected the bioenergetic status of ASC in which both the maximum oxygen consumption rate and extracellular acidification rate were decreased. This was corroborated by a reduced uptake of glucose under HG. In spite of these observations, in vitro, ASC promoted the formation of vascular-like networks of human umbilical vein endothelial cells on monolayers of ASC under HG with minimally affected.

Introduction

The International Diabetes Federation estimates that there were 366 million people living with diabetes in 2011; by 2030 this will have increased to 552 million [1]. Diabetes enhances the risk of clinical ophthalmologic complications and particular of diabetic retinopathy (DR), which is the main cause of blindness in the working-age population of developed countries [2]. DR is the result of a disordered glucose metabolism and is characterized by the early loss of two main cell types of retinal capillaries: the pericyte, which wraps capillaries and the endothelial cell [3]. Pericytes are derived from the vascular smooth muscle lineage and exist in contact with endothelial cells. Pericytes provide a nourishing, anti-inflammatory and antiangiogenic environment for endothelial cells that makes them a potential mediator of the functional blood–retinal barrier, which is dependent on the interaction of the vascular endothelial cells with both glial cells and pericytes [4,5]. The onset of DR is caused by intracellular accumulation of reactive oxygen species (ROS) that are induced by hyperglycemia (HG). The ROS induces apoptosis of pericytes, which exacerbates capillary death. The formation of acellular capillaries and pericyte ghosts are typically the first abnormalities that are observed clinically in DR [6]. The capillary degeneration causes substantial ischemia and local hypoxia, which triggers massive neovascularization, typical for later stages of retinopathy [7]. In the absence of pericytes, these new vessels are not quiescent and do not mature, while the angiogenesis process continues. The resulting capillaries are morphologically and functionally abnormal. In particular, their high permeability causes leakage of serum and cellular components into the vitreous. If the condition is not diagnosed and treated, the increased pressure can eventually lead to blindness [8,9]. Therefore, during DR the retina is in demand of a suitable cellular replacement for pericytes. It is well recognized that in HG the electron transport chain is overwhelmed with substrate and starts to produce oxygen radicals that is, ROS [10]. Exacerbated ROS may induce the opening of the permeability transition pore, creating swollen mitochondria. These swollen mitochondria may present rupture in the mitochondrial outer membrane and leak out cytochrome c, calcium ions to mention a few and cause both apoptosis and necrosis. Through these effects, oxidative stress together with the downregulation of antioxidative enzymes play an important role in the pathogenesis of DR [11,12]. The early stage of

[1]Department of Pathology and Medical Biology, University Medical Center Groningen, University of Groningen, Groningen, the Netherlands.
[2]Millennium Institute of Immunology and Immunotherapy, Santiago, Chile.
[3]Faculty of Biological Sciences and Faculty of Medicine, Center for Biomedical Research, Universidad Andres Bello, Santiago, Chile.
[4]Department of Pediatrics and Laboratory Medicine, Center for Liver, Digestive and Metabolic Diseases, University Medical Center Groningen, University of Groningen, Groningen, the Netherlands.

retinopathy (non-proliferative retinopathy) frequently goes unnoticed as it does not have significant pathological signs. However, advanced retinopathy (proliferative retinopathy) is in high demand of treatment, due to the existence of leaky, nonfunctional, and highly proliferative vessels that require normalization of blood glucose levels, laser treatment, vitrectomy, and injection of an anti-VEGF (vascular endothelial growth factor) medicine combined with anti-inflammatory medicine to name a few. All these methods no more than partially prevent or delay loss of vision. More importantly, replacement pericytes are required to blunt the ongoing proliferative angiogenesis while normalizing the capillary function. This is not possible to date. Promising results from animal models and recent in vitro studies have been published that will impact DR via a regenerative medicine-based approach over the coming years [13,14]. Adipose tissue-derived stromal cells (ASC) are abundant, accessible multipotent mesenchymal stromal cells that can be easily isolated from human adipose tissue. ASC have been recently shown to have functional and phenotypic overlap with pericytes covering micro-vessels in adipose tissues [15]. ASC and pericytes share the same surface markers including NG2, CD140a, and CD140b (PDGFR α and β). Also, human ASC cooperate with endothelial cells to form vascular-like networks in vitro [15,16]. It has been shown that in a rodent model for chronic diabetes, ASC acquired pericytic features, which rescued proliferative angiogenesis in the retina under hyperglycemic conditions [17]. Importantly, these studies suggested the direct role of ASC in providing retinal microvascular support and appear to migrate and integrate with the retinal microvasculature [17,18]. ASC features may allow a functional replacement, at least short term, pericytes loss in DR. While retinal pericytes readily undergo HG and ROS-driven apoptosis, it is unclear why ASC that engraft diabetic retinal vasculature appear refractory to HG.

In this study, we investigated the influence of HG on the mitochondrial function and metabolic activity of ASC and on their pericytic function in vitro. This information may help to delineate both their capabilities and limitations with respect to their potential clinical translation.

Material and Methods

Cell isolation and culture

Human subcutaneous adipose tissue samples from healthy human subjects with body mass index <30 were obtained after liposuction surgery (Bergman Clinics). All donors provided informed consent and all procedures were performed in accordance to national and institutional guidelines as well as with the ethical rules for human experimentation stated in the Declaration of Helsinki.

For ASC isolation, lipoaspirates were enzymatically digested with 0.1% collagenase A (Roche Diagnostic) in phosphate-buffered saline (PBS), containing 1% bovine serum albumin (Sigma-Aldrich) at 37°C for 90 mins. Centrifugation (300 *g*, 4°C, 10 mins) was used to separate adipocytes and lipid content from the stromal cell fraction. The stromal cell fraction was subjected to Lymphoprep (Axis-Shield PoC) density gradient centrifugation. The cells from the interface were seeded in culture flasks at 10,000 cells/cm^2. The culture medium was normoglycemic RPMI-1640 (5 mM D-glucose, NG-RPMI) (Lonza Biowhittaker Verviers) supplemented with 10% fetal bovine serum (FBS) (Thermo Scientific), 100 U/mL penicillin, 100 µg/mL streptomycin (Gibco, Life Technologies), and 2 mM L-glutamine (Lonza Biowhittaker Verviers). It was sterilized by filtration (0.22 µm). Optimal culture conditions of 37°C, 5% CO2, and 95% humidity were maintained throughout the culture period. ASC in passage 1–3 were harvested with Trypsin-EDTA in 0.9% NaCl (Sigma-Aldrich) and routinely checked for both mesenchymal cell surface and pericyte markers, including CD31–/CD44+/CD45–/CD29+/CD105+/CD144–/NG2+/PDGFRβ+ [19]. The cells were passaged at 70%–80% confluence until passage3 (P3) with three changes of medium per week. The cells from P3–6 were cultured in normoglycemic and hyperglycemic (30 mM D-glucose, HG-RPMI) conditions. An osmotic control medium made of 5 mM D-glucose plus 25 mM mannitol (NG+Ma-RPMI) of RPMI-1640 was also used. Cell culture medium was changed daily during the 7 days of the experiment. The pooled ASC from three different donors were used for the experiments of this study. Human Umbilical vein endothelial cells (HUVEC) were cultured on gelatin-coated culture flasks at 10,000 cells/cm^2 in endothelial culture medium (ECM) consisting of medium NG-RPMI medium supplemented with 10% FBS, 100 U/mL penicillin, 100 µg/mL streptomycin, 2 mM L-glutamine plus 5 U/mL heparin (Leo Pharma), and 50 µg/mL of endothelial cell growth factor [20]. For the cocultures of ASC and HUVEC, ASC had to be cultured in RPMI-based medium, the influence of DMEM-based and RPMI-based medium on the expression of mesenchymal and pericytic markers in ASC was assessed (Supplementary Fig. S1; Supplementary Data are available online at www.liebertpub.com/scd). The expression of PDGFRβ, NG2 were marginally reduced in long-term cultures of ASC in ECM and considered of no influence to the experiments.

Immunofluorescence analysis of cocultured ASC and HUVEC

ASC were plated in 24-well cell culture plates (Corning) at 10,000 cells/cm^2 in NG-RPMI medium for 5 days. HUVEC were seeded on top of ASC monolayers or as the control on gelatin-coated wells at 10,000 cells/cm^2 in NG-ECM or HG-ECM for 7 more days after which vascular networks had formed. Cells were washed with PBS and fixed in 2% paraformaldehyde in PBS at RT for 20 min. Cells were permeabilized with 0.5% Triton X-100 in PBS (Sigma-Aldrich) for 15 min. Subsequently, samples were incubated with goat-anti-human-RGS5 antibody (1:100; Santa Cruz)/rabbit anti-human-SM22α antibody (1:100; Abcam) and mouse-anti-human-CD31 antibody (1:100; Dako) for 90 min. Samples were washed with PBS and incubated with a cyanine3-conjugated-rabbit-antibody to goat-IgG for RGS5/cyanine3-conjugated-donkey-antibody to rabbit-IgG for SM22a (1:300; Life Technologies) and fluorescein-conjugated-donkey-antibody to mouse-IgG (for CD31, 1:300; Life Technologies) for 45 min. Stained samples were mounted with PBS. Imaging was performed with a high-end fully motorized Zeiss AxioObserver Z1 epifluorescent microscope (TissueGnosticsTissue Faxs). The coculture experiment was repeated with HUVEC that were lentivirally tagged to express EGFP (green) and ASC lentivirally tagged with dTomato (red) to monitor the origin cells irrespective of phenotypes changes during coculture.

Apoptosis and proliferation

To estimate the influence of HG on cell survival, apoptosis was evaluated by fluorescence-activated cell sorting (FACS) analysis using an Apoptotic/Necrotic Cells Detection Kit (PromoKine). Briefly, ASC were treated with NG-RPMI, HG-RPMI, and NG+Ma-RPMI medium for 7 days and harvested by Trypsin-EDTA in 0.9% NaCl right after treatment. Cells were washed with PBS once and resuspended in 500 μL kit binding buffer (100,000 cells/500 μL) and stained in the dark with 2.5 μL FITC-AnnexinV (marker for apoptosis) and 2.5 μL of Ethidium Homodimer lll (marker for necrosis) at RT for 15 min. Samples were analyzed using a FACS Calibur flow-cytometer (BD biosciences) within 1 h after staining and the results were analyzed with Kaluza 1.2 software. For measurement of proliferation, ASC from P3-6 were plated on 24-well cell culture plates (Corning) at 10,000 cells/cm^2 in NG-RPMI medium with 10% FBS for 24 h. The medium was changed for NG-RPMI, HG-RPMI, or osmotic control, all with 5% FBS for 7 days. Medium was changed daily. Cells were fixed and permeabilized as described above. Samples were incubated with rabbit-anti-human-ki67 (Monosan PSX1028) 1:250 in DAPI (5 mg/mL; Sigma-Aldrich) for 90 min. Samples were washed and subsequently stained by incubation with a cyanine3-conjugated-donkey-antibody to rabbit-IgG (1:100; Life Technologies) for 30 min. Stained samples were mounted with PBS. Imaging was performed with a high-end fully motorized Zeiss AxioObserver Z1 epifluorescent microscope.

Detection of ROS level

Cellular ROS production was determined using the dye 2′,7′-dichlorofluorescein diacetate (DCFH-DA; Sigma-Aldrich), a cell permeable nonfluorescent probe, which is de-esterified intracellularly by means of esterases (DCFH) and turns to highly fluorescent 2′,7′-dichlorofluorescein (DCF) on oxidation [21]. Cells were harvested after 7 days culturing in NG, HG, and NG+Ma-RPMI medium and suspended in 1 mL of medium followed by incubation with 20 μM DCFH-DA in the dark at 37°C for 15 min. Samples were analyzed directly without washing using a FACS Calibur flow cytometer (BD Biosciences) within 15 min after the staining and the results were analyzed with Kaluza 1.2 software.

Assessment of mitochondrial membrane potential and mitochondrial morphology analysis

To specify the influence of HG on mitochondrial morphology and membrane potential, ASC cultured in NG-RPMI or HG-RPMI medium for 7 days were incubated at 37°C in a 5% CO2 humidified chamber with 120 nM membrane potential–independent dye MitoTracker Green FM (MTG, Green, Life Technologies) and 10 nM tetramethylrhodamine, ethyl ester, perchlorate (TMRE, Red-orange; Life Technologies), a membrane potential-dependent fluorescent dye for 45 min, washed three times, and incubated in medium containing TMRE for 15 min before imaging to allow adequate equilibration of the membrane potential-sensitive TMRE dye within the mitochondria. TMRE was kept in the medium while imaging. All experiments were performed in triplicate with at least three technical replicates and normalized by the number of cells per sample.

Confocal microscopy

Cells were imaged live by confocal microscope (Leica TCS SP8 Confocal Microscope) with a 63 × oil immersion objective. The cells were kept at 37°C in a 5% CO2 humidified microscope stage chamber. MTG was subjected to 490 nm argon laser excitation and 516 nm filter emission. TMRE was recorded through a band-pass 573–607 nm filter. To observe individual mitochondria Z-stack images were acquired in series of six slices per cell ranging in thickness from 0.5 to 0.8 μm per slice [22].

Analysis of mitochondrial length and circularity

Mitochondrial circularity of ASC was measured as described previously [23]. Mitochondrial circularity is a measure of ''roundness'' of mitochondria with 0 referring to a straight line and 1 as a perfect circle. Cells containing a majority of long interconnected mitochondrial networks were classified as cells with tubular mitochondria. Cells with a majority of short mitochondria were classified as fragmented and cells with mostly sparse small round mitochondria were classified as very fragmented [24]. Morphological aspects were measured by ImageJ software for individual mitochondria.

Oxygen consumption rate and extracellular acidification rate

The oxygen consumption rate (OCR) and extracellular acidification rate (ECAR) of ASC grown in NG-RPMI or HG-RPMI medium were measured by a bioenergetic assay (XF24; Seahorse Bioscience). ASC were plated and grown on V7-PS plate (Seahorse Bioscience, Inc.) in NG-RPMI or HG-RPMI medium to reach a confluent monolayer for 7 days. Assays were initiated by removing growth medium, replacing with unbuffered RPMI-1640 medium and incubating at 37°C for 60 min in a CO2-free incubator to allow temperature equilibrium and CO2 degassing from plate. The microplate was then assayed (XF24 Extracellular Flux Analyzer; Seahorse Bioscience) to measure extracellular flux changes of oxygen and pH in the medium immediately surrounding the adherent cells. After steady state measurement, oxygen consumption and ECARs were obtained. Oligomycin (2 μM), which inhibits ATP synthase, and the proton ionophore FCCP [carbonyl cyanide 4-(trifluoromethoxy) phenylhydrazone; 5 μM], which uncouples mitochondria, were injected sequentially through reagent delivery chambers for each well in the microplate, to obtain maximum OCRs. Finally, a mixture containing 2 μM rotenone (an inhibitor of mitochondrial complex I) and 2 μM antimycin A (an electron transport blocker) was injected to confirm that respiration changes were mainly due to mitochondrial respiration. The values of oxygen consumption and extracellular acidification were normalized to total cellular proteins in each sample well.

Assessment of glucose uptake by 2-deoxy D-glucose

To determine the influence of HG on glucose uptake in ASC, cells from P3–6 were cultured in NG or HG for 7 days. After that cells were washed twice with PBS and serum deprived for 4 h, in either NG or HG medium supplemented with 100 U/mL penicillin, 100 μg/mL streptomycin, and 2 mM L-glutamine.

Subsequently, the ASC were stimulated with 100 nM insulin (Novorapid; Novo Nordisk) for 20 min at 37°C or left untreated. The medium was removed, cells were washed twice with warm PBS, and 1 mL of PBS containing 0.1 μCi 2-deoxy-D-[14C]glucose (14C-2-DOG) (Perkin Elmer) and unlabeled 2-deoxy-D-glucose (2DG) (100 μM; Sigma-Aldrich) was added to each well. The uptake reaction was carried out at 37°C for 45 min. Glucose transport was terminated by washing twice with ice-cold PBS. Cells were harvested and lysed in 0.5 mL 0.05M NaOH. Of this, a 400 μL aliquot was used for β-scintillation determination by addition of scintillation cocktail and subsequent scintillation determination in a β-scintillation counter. The remaining 100 μL were used for the determination of protein concentration with the Pierce™ BCA Protein Assay Kit (Life Technologies). The results were analyzed as 2DG uptake in pmol/μg of protein. The data are plotted as the fold change in 2DG uptake after culturing in HG compared to culturing in NG.

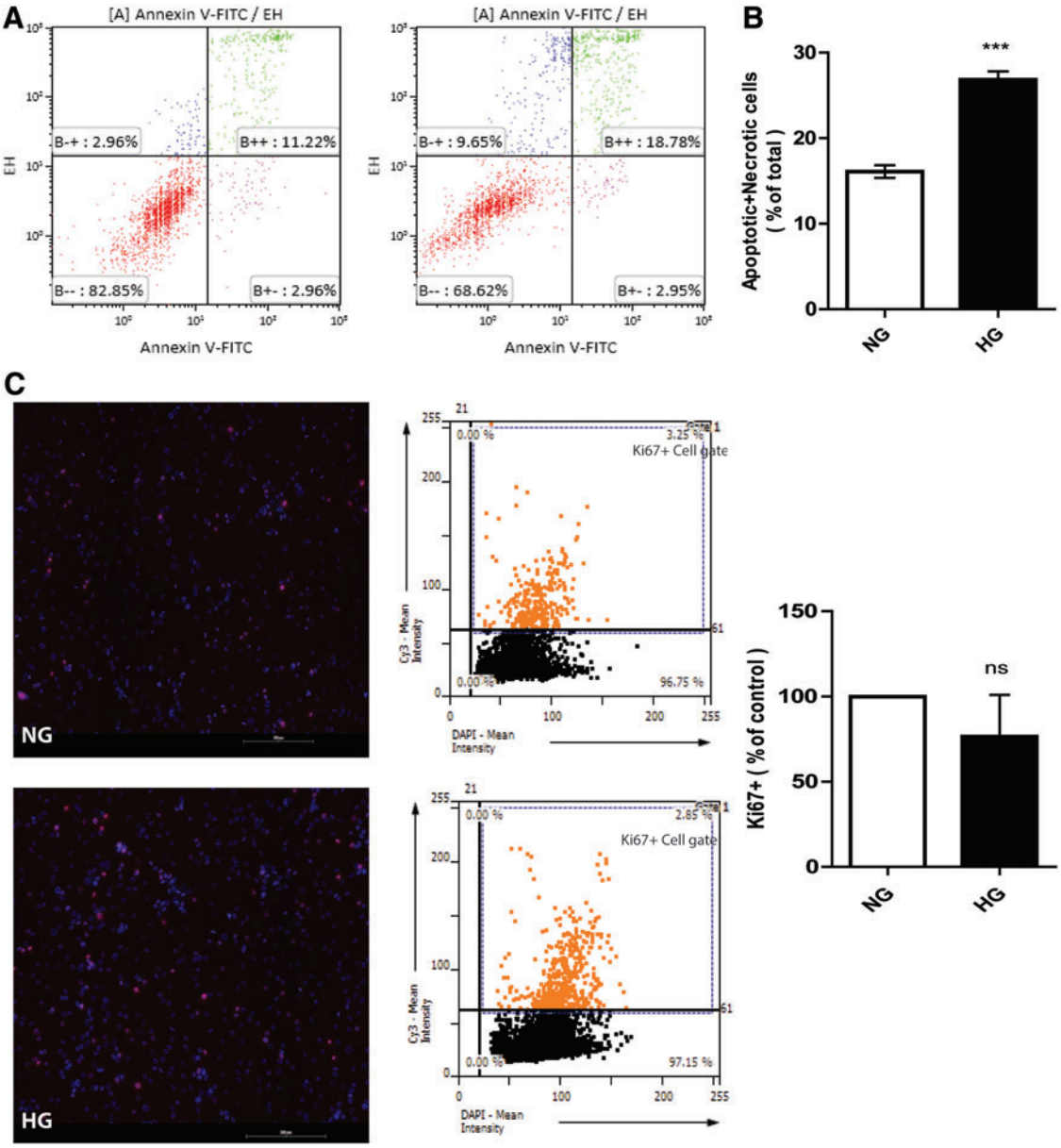

FIG. 1. ASC undergo apoptosis after exposure to HG for 7 days. Apoptosis and necrosis were quantified by FACS after FITC-Annexin V and Ethidium Homodimer lll labeling. **(A)** Representative FACS data for ASC in NG and HG. The abscissa and ordinate represent the fluorescence intensity of Annexin V and Ethidium Homodimer lll, respectively. **(B)** Bar graph represents the mean percentage of the total apoptosis and necrosis rate ± SEM. ($n = 5$). (***$P < 0.0001$) **(C)** Proliferation of ASC is not influenced after exposure to HG for 7 days. Immunofluorescent staining of Ki67 (proliferation marker) after 7 days of culture in NG or HG medium. Images were analyzed with TissueGnostics tissue FAXS software. The bar graph shows the percentage of positive ki67 cells in HG-medium to the control (NG-medium culturing). The data are presented as the mean ± SEM. Scale bar = 200 μm. ASC, adipose tissue-derived stromal cells; FACS, fluorescence-activated cell sorting; NG, normoglycemia; HG, hyperglycemia. Color images available online at www.liebertpub.com/scd

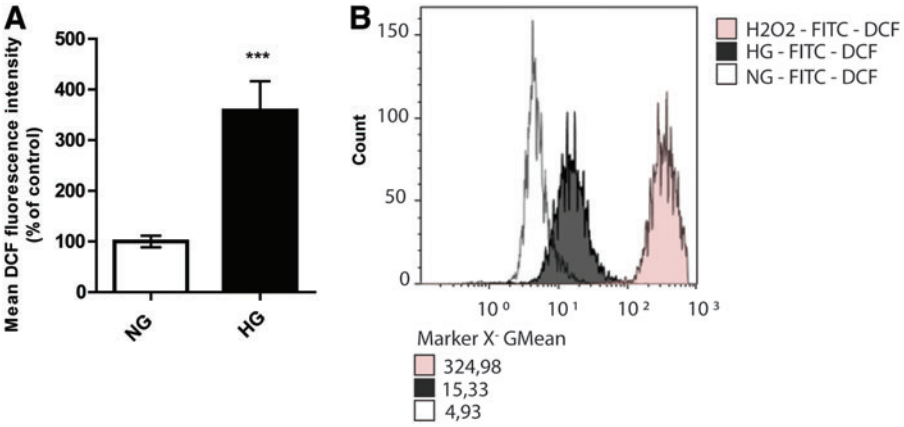

FIG. 2. HG induces production of total cellular ROS in ASC. ROS production was measured by conversion of DCF in ASC after exposure to HG for 7 days. **(A)** The flow cytometric analysis shows a significantly higher mean fluorescence intensity (MFI) in HG compared to NG (***$P < 0.0001$). The graphs show the mean ± SEM ($n = 8$). **(B)** The histograms shows the representative increase of mean intensity after exposure to HG or H2O2 control compared to NG. ROS, reactive oxygen species. Color images available online at www.liebertpub.com/scd

Statistics

All the data are presented as a mean ± SEM and were analyzed by GraphPad Prism (GraphPad Software, Inc.). Statistical significance was determined using one-way ANOVA and unpaired t-test analysis. Values of $p < 0.05$ were considered statistically significant.

Results

HG reduces viability of ASC, but does not influence proliferation

After 7 days culture in HG medium ~25% ± 1.1% of the ASC were apoptotic and necrotic, while this was reduced in NG (16% ± 0.8%, $P < 0.0001$, Fig. 1A, B). Interestingly, the level of proliferation, as determined by the fraction of Ki-67-expressing ASC, did not differ between cells cultured in NG medium versus HG medium (Fig. 1C) or osmotic controls (data not shown) after 7 days culture.

HG induces ROS in ASC

ASC cultured in NG or control medium produced virtually no ROS, as determined by FACS analysis of converted DCFH-DA. However, 7 days culture of ASC in HG medium increased intracellular levels of ROS by more than threefold ($P < 0.0001$, Fig. 2A). In the positive control cells which were treated with 1 mM hydrogen peroxide (Merk) as a potent ROS inducer, ROS induced well beyond the levels induced by HG (Fig. 2B).

HG alters the mitochondrial membrane potential and changes the mitochondrial phenotype of ASC

The continuous culture of ASC in HG medium decreased their mitochondrial membrane potential by ~31% ± 8% compared to NG medium as judged by TMRE fluorescence ($P < 0.001$, Fig. 3). This apparent sign of a decreased mitochondrial membrane potential was corroborated by disturbances in the mitochondrial network of ASC cultured in HG medium for 7 days and assessed with MitoTracker dye. This showed a significant decrease of 23% ± 9.6% compared to the NG control. ASC cultured in NG medium had an extensive network of mitochondria throughout the cell ($P < 0.01$, Fig. 4A). Another relevant feature to determine mitochondrial dysfunction is mitochondrial shape and circularity. We observed a mainly tubular mitochondrial morphology in the ASC cultured in NG medium, which changed to a fragmented morphology when cultured in HG medium for 7 days. The mitochondrial fragmentation increased to virtually small fragments in nonphysiologically high (50 mM) glucose concentrations ($P < 0.0001$, Fig. 4B).

HG decreases the maximum OCR and the ECAR in ASC

ASC cultured in NG or HG conditions were simultaneously measured with a bioenergetic assay (XF24; Seahorse Bioscience) to determine the rates of cellular oxygen consumption and extracellular acidification. Steady state of oxygen consumption and extracellular acidification were measured at three time points (Fig. 5). Oligomycin (Fig. 5A:

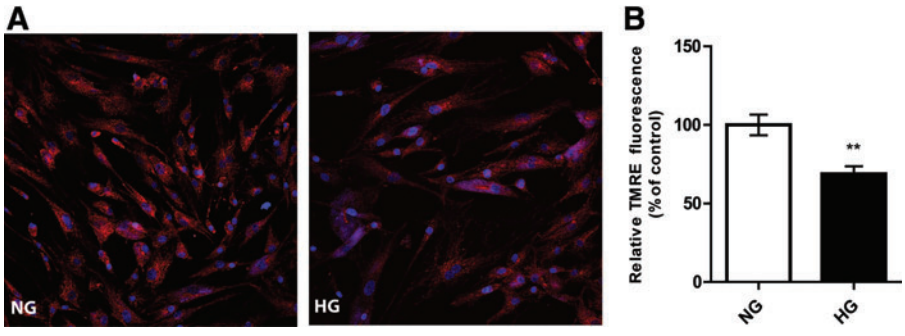

FIG. 3. HG effected mitochondrial membrane potential of ASC. **(A)** Mitochondrial membrane potential of ASC grown for 7 days in NG or HG medium was detected and measured with mitochondrial membrane potential–sensitive TMRE (*red*) dye using confocal laser scanning microscopy. **(B)** The results were plotted as MFI ± SEM (**$P < 0.001$). Color images available online at www.liebertpub.com/scd

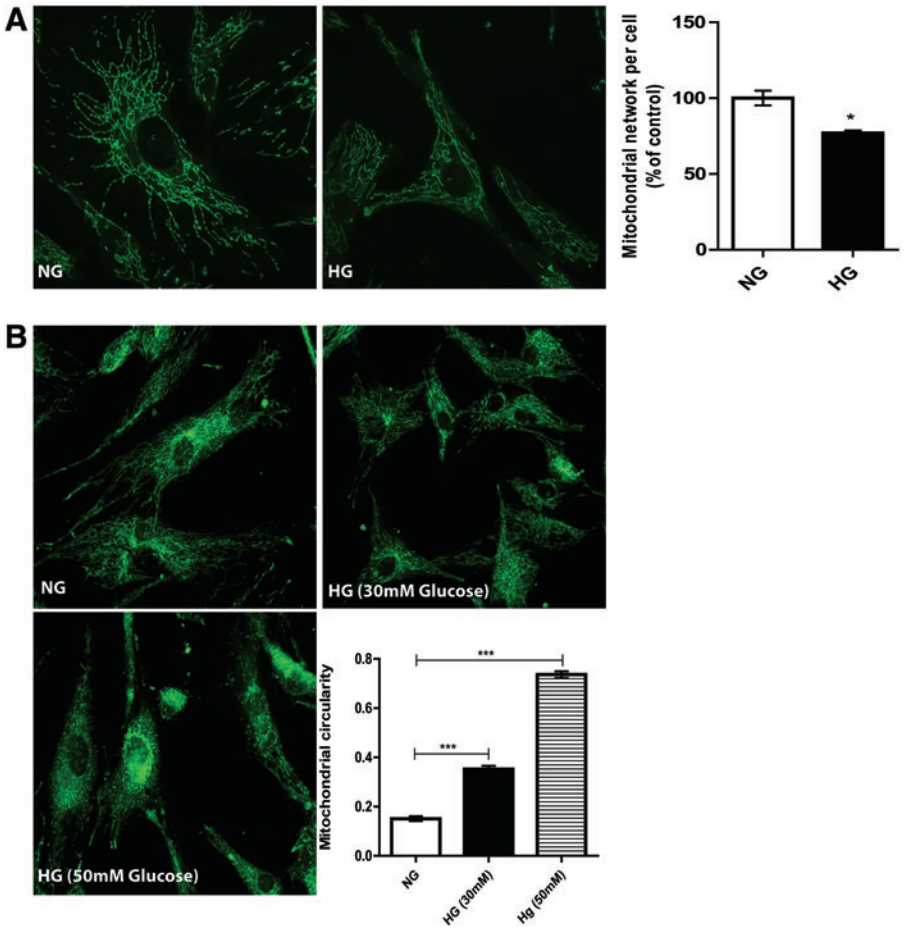

FIG. 4. Mitochondrial morphology of ASC changes after exposure to HG. **(A)** Confocal images of ASC cultured in NG medium stained with membrane potential– independent dye MitoTracker Green FM show a network of interconnected, long and tubular mitochondria. HG significantly disrupts these mitochondrial networks. (*$P < 0.01$) **(B)** HG induces mitochondrial fragmentation in ASC in a dose-dependent fashion. Compared to normoglycemic controls, the exposure of ASC to 30 mM glucose more than doubles the circularity (measure of fragmentation) of mitochondria, which increases another twofold when exposed to 50 mM glucose. ± SEM (***$P < 0.0001$). Color images available online at www.liebertpub.com/scd

injection vertical line A) was injected to inhibit ATP synthase, followed by the addition of FCCP (Fig. 5A: injection vertical line B) to uncouple mitochondria and obtain values for maximum oxygen consumption. Finally, mixture of rotenone and antimycin A were injected (Fig. 5A: injection vertical line C) to confirm that the respiration changes just could be attributed to mitochondrial respiration. ASC grown in HG showed a significant decrease (29.54% ± 3%) in maximum oxygen consumption compared to ASC grown in NG medium ($P < 0.0001$, Fig. 5B). ECARs were examined simultaneously. Changes in the ECAR may indicate changes in the rate of glycolysis in these cells. Under HG, ASC showed significantly decreased extracellular acidification (Basal: 10%, oligomycin-induced: 34%, and FCCP-induced: 44%) as compared with ASC grown in NG medium ($P < 0.01$, Fig. 5C).

HG affects the glucose metabolism of ASC

Measuring uptake of 2DG is the gold standard to assess glucose uptake. ASC cultured in HG showed a 41% ± 0.17% decrease in glucose uptake compared to NG medium cultured ASC ($P < 0.01$, Fig. 5D), which is in line with the results from the extracellular acidification measurements. In mature adipocytes insulin stimulates the uptake of glucose into these cells. ASC can be regarded as the precursors of adipocytes. Interestingly, in our experiments insulin did not affect the glucose uptake into ASC. This shows that under these conditions ASC are not sensitive to insulin in terms of increased glucose uptake. Yet, *GLUT4*, the insulin-sensitive glucose transporter, was normally expressed (data not shown).

The stimulation by ASC of vascular networks of HUVEC in vitro is affected by HG

In NG medium, preformed monolayers of ASC promoted the formation of vascular network-like structures by seeded HUVEC during 7 days coculture (Fig. 6A). These networks were absent in ASC or HUVEC controls (data not shown). The vascular-like networks comprise of interconnected multicellular tubes of endothelial cells with a lumen ranging from capillary size to multicellular structures to which ASC attach in a pericytic fashion as shown by their pericytic position and expression of SM22α (Fig. 6B, Supplementary Video S1). This is corroborated by the absence of SM22α expression by the ASC that are not involved in vascular stabilization that is, which remained bound to the tissue culture plate itself (Fig. 6B). In HG medium, the ASC still supported the formation of vascular networks by HUVEC, although at a 29% ± 3.5% reduced scale ($P < 0.0001$, Fig. 6C).

Discussion

DR is characterized by progressive alterations in the retinal microvasculature, increasing vascular permeability caused by apoptosis in endothelial cells, and pericyte loss

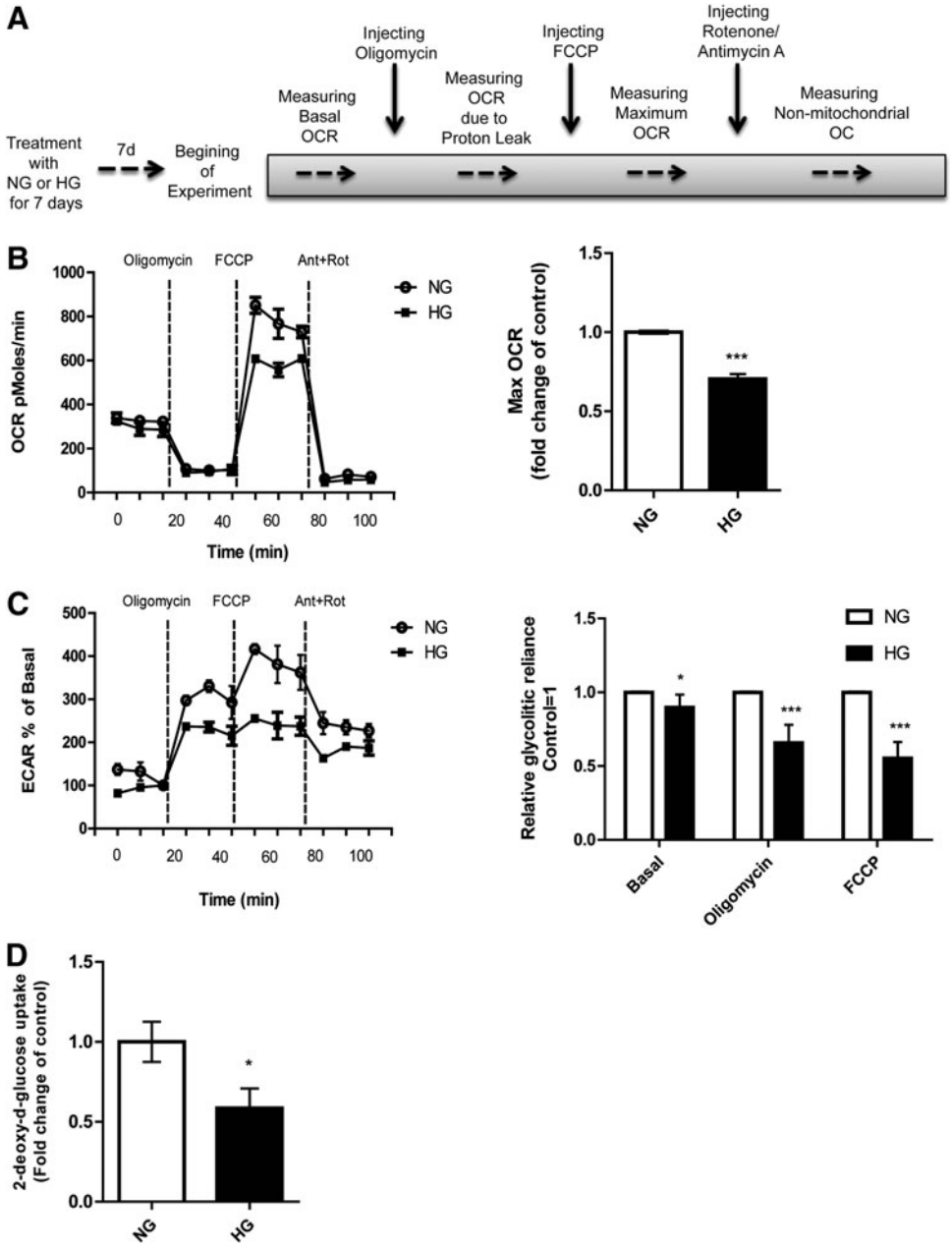

FIG. 5. HG affects mitochondrial maximum oxygen consumption rate (OCR) and extracellular acidification in ASC. **(A)** Protocol for assessing mitochondrial function in ASC after exposure to HG. After measuring the basal respiration rate of cells, compounds modulating mitochondrial function are added sequentially. The effect on OCR and ECAR are measured after each compound addition. **(B)** The line graph shows the experimental evaluation of steady state and maximum OCR for ASC grown in NG or HG 7 days (NG: *open circles* -○-, HG: *black squares* -■-). *Dotted lines* **(A–C)** indicate injections of oligomycin, FCCP, and rotenone/antimycin A, respectively. The exposure of ASC to HG for 7 days results in reduced maximum OCRs compared to normoglycemic controls. (***$P < 0.0001$) **(C)** HG reduces the extracellular acidification rate of ASC in basal state and also after inhibiting ATP synthase by oligomycin (after *dotted line* A) and injection of FCCP, which uncouples mitochondria (after *dotted line* B). (*$P < 0.01$, ***$P < 0.0001$) **(D)** HG significantly decreases the uptake of labeled 2-deoxyglucose by ASC. Figure shows the rate of glucose uptake, measured as pmol per μg protein and presented as the fold change compared to the control ± SEM. ($n = 9$). In all cases the scored data were normalized for protein content (*$P < 0.01$).

that leads to abnormal neovascularization in the late stage of the disease [25,26]. Consequently, pericyte replacement would be an important step in the treatment or reversal of DR. Although, ASC are pericyte-like cells and they would be promising to stabilize the vessels in DR, more studies are necessary to show the mechanism of ASC in interaction with endothelial cells in DR in vivo. In this study we showed the influence of HG on these cells in vitro individually. HG has a remarkable influence on retinal pericyte and retinal endothelial cells including bioenergetics and metabolic dysfunction, reduced mitochondrial function, and induced mitochondrial fragmentation [22,27]. The detrimental effects of HG on mitochondrial function and cellular metabolism could play a role in the apoptosis associated with the retinal pericytes and endothelial cells in DR [28]. We showed ASC had increased intracellular ROS after a long-term (7 days) exposure to HG. Chronic HG caused mitochondrial dysfunction in ASC, which was observed both as a decreased membrane potential in HG and as structural changes as well. The increased ROS production correlated with increased apoptosis and necrosis of ASC. Interestingly, the proliferation capacity of ASC after exposure to HG for 7 days was not affected. This indicates that, with respect to function, ASC are largely refractory to the mitochondrial dysfunction that is induced by HG in vitro. It is well known that HG-induced overproduction of ROS can disrupt the mitochondrial membrane potential and damage appropriate functioning of the mitochondria [29]. This deviation in mitochondrial function is an early sign of apoptosis, which was confirmed by the apoptosis increased in treated cells [30,31]. We showed that ASC, similar to most mammalian cell types in NG, form long and tubular

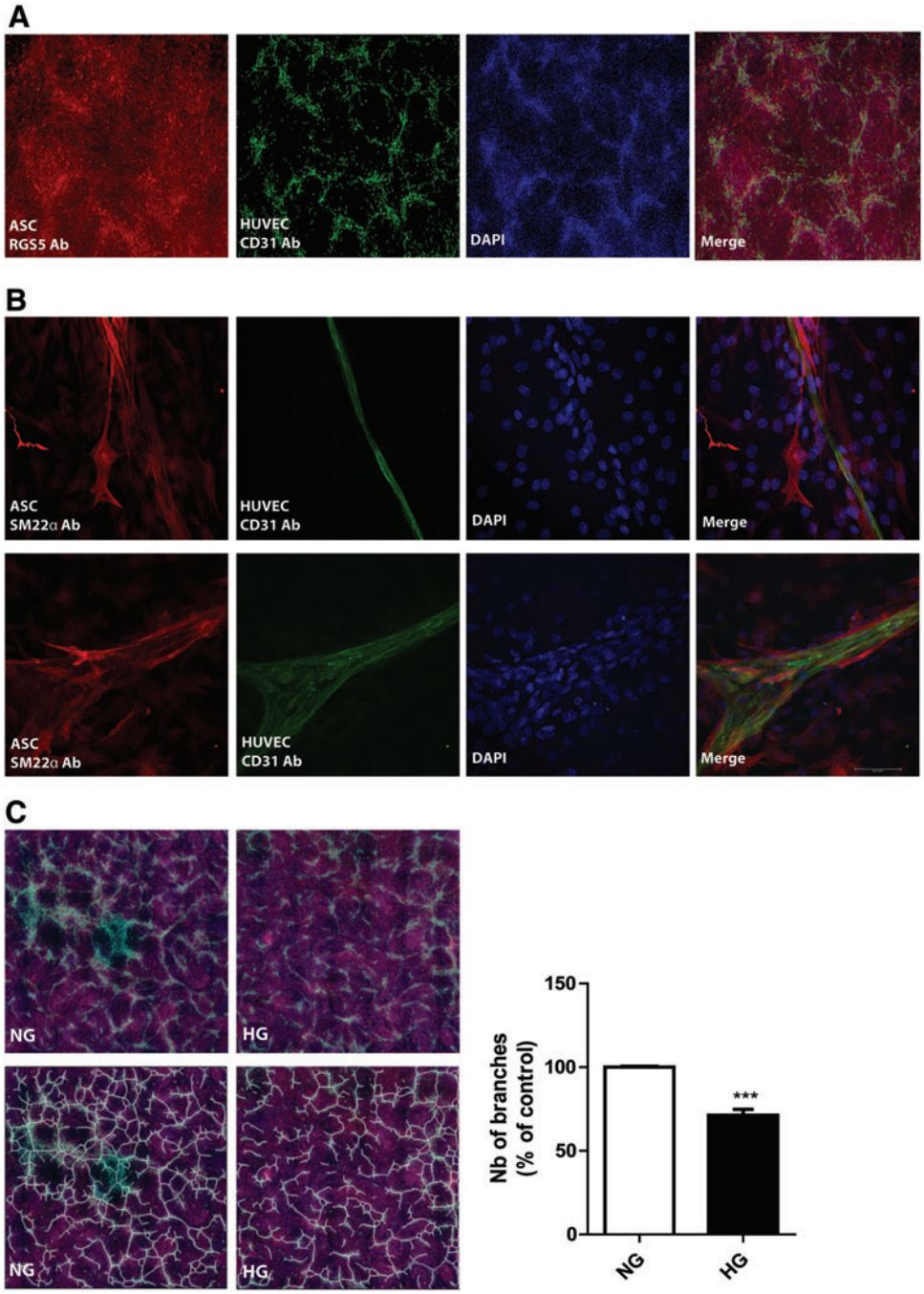

FIG. 6. **(A)** HUVEC (CD31, *green*) seeded on top of a monolayer of ASC (RGS5, *red*) for 7 days, results in the formation of vascular network-like structures, which does not occur in monolayers of HUVEC and ASC separately. **(B)** High resolution (63×) imaging using confocal laser scanning microscopy of interactions of ASC with vascular-like networks of HUVEC (*green* CD31). These vascular-like networks comprise of interconnected multicellular tubes of endothelial cells with a lumen ranging from capillary size to multicellular structures to which ASC attach in a pericytic fashion as shown by their pericytic position and expression of SM22α (*red*). Nuclei—*blue* (DAPI) **(C)** HG decreases the number of branches in vascular networks on the monolayer of ASC. The network formation was analyzed with the ImageJ angiogenesis analyzer for each well (growth area 1.9 cm^2) and the number of branches were compared with the control condition (NG) (***$P < 0.0001$). HUVEC, human umbilical vein endothelial cells. Color images available online at www.liebertpub.com/scd

networks of mitochondria. These networks are critical for a normal function of the mitochondria by regulation of fusion and fission events that involve the formation or breaking of the mitochondria network, respectively [32]. A decrease in the rate of fusion and a simultaneous increase in the rate of fission cause fragmentation of the mitochondrial network, which results in shorter and rounder mitochondria [33]. Our results suggest that HG-induced mitochondrial fragmentation maybe involved in the increased ROS production in ASC. It remains unclear, however, why the proliferation rate of ASC was unaffected by ROS production under HG. While mitochondria are functional, they support cell proliferation. The fact that mitochondria under HG display similar basal respiration as NG, means that HG cells can deal with the stress condition. However, they are still suffering from HG according to the statement that maximal respiration is decreased and losing their capacity to make ATP. Our results indicate that HG caused a decrease of the maximal OCR and the rate of extracellular acidification. The basal level of extracellular acidification in ASC decreased during HG exposure, and also after incubation with ATP synthase inhibitor (Oligomycin) and mitochondria uncoupler (FCCP). Corroborating the data obtained from the flux analyses, HG caused a significant decline in glucose uptake in ASC. Interestingly, this diminished rate of glycolysis was unresponsive to insulin

stimulation. Our results indicate that ASC cultured in HG compensate the hyperglycemic environment by changing the metabolic capacity, as displayed by decreased oxygen consumption and glycolysis.

In this study the question was addressed how the chronic diabetic microenvironment affects the ASC's therapeutic potential. This was investigated through continuous exposure of HG on ASC and their capacity to support the formation of vascular networks by HUVEC. Interestingly, the networks were still formed, although with a reduced number of branches. The ROS-induced mitochondrial dysfunction and apoptosis, only partly affected the pericytic function of ASC, because network formation by endothelial cells was only marginally affected. Our in vitro results corroborate published data that ASC could functionally engraft in the retinal vasculature of hyperglycemic mice [17,18], while providing part of the protective measurements taken by HG-exposed ASC. Taken together, our results suggest ASC are largely resistant to long-term exposure to HG, which would explain why ASC can acquire a pericytic function in the diabetic retinal vasculature in mouse models for DR. Our current research focuses on the paracrine and juxtacrine interactions between pericytic ASC and retinal microvascular endothelial cells under HG to understand how ASC protect microvascular endothelial cells and promote their vascular stabilization.

Acknowledgments

TissueGnostics tissue FAXS, Austria, which is sponsored by NWO-grants 40-00506-98-9021. Additional funding: Cochilco-Fondecyt 1100995 (AAE), IMII P09-016-F (AAE). FP7 program:EULAMDIMA (PIRSES-GA-2011-295185). Dutch Diabetes Foundation (2012.00.1537). The skillful technical assistance of K.A. Sjollema is greatly acknowledged.

Author Disclosure Statement

No competing financial interests exist.

References

1. Whiting DR, L Guariguata, C Weil and J Shaw. (2011). IDF diabetes atlas: global estimates of the prevalence of diabetes for 2011 and 2030. Diabetes Res Clin Pract 94: 311–321.
2. Centers for Disease Control and Prevention (CDC). (1996). Blindness caused by diabetes—Massachusetts, 1987–1994. MMWR Morb Mortal Wkly Rep 45:937–941.
3. Hammes HP, J Lin, O Renner, M Shani, A Lundqvist, C Betsholtz, M Brownlee and U Deutsch. (2002). Pericytes and the pathogenesis of diabetic retinopathy. Diabetes 51: 3107–3112.
4. Armulik A, A Abramsson and C Betsholtz. (2005). Endothelial/pericyte interactions. Circ Res 97:512–523.
5. Rajashekhar G. (2014). Mesenchymal stem cells: new players in retinopathy therapy. Front Endocrinol (Lausanne) 5:59.
6. Kowluru RA, J Tang and TS Kern. (2001). Abnormalities of retinal metabolism in diabetes and experimental galactosemia. VII. Effect of long-term administration of antioxidants on the development of retinopathy. Diabetes 50:1938–1942.
7. Cai J and M Boulton. (2002). The pathogenesis of diabetic retinopathy: old concepts and new questions. Eye (Lond) 16:242–260.
8. Henkind P and GN Wise. (1974). Retinal neovascularization, collaterals, and vascular shunts. Br J Ophthalmol 58:413–422.
9. Bergers G and S Song. (2005). The role of pericytes in blood-vessel formation and maintenance. Neuro Oncol 7: 452–464.
10. Green K, MD Brand and MP Murphy. (2004). Prevention of mitochondrial oxidative damage as a therapeutic strategy in diabetes. Diabetes 53 Suppl 1:S110–S118.
11. Kowluru RA and PS Chan. (2007). Oxidative stress and diabetic retinopathy. Exp Diabetes Res 2007:43603.
12. Madsen-Bouterse SA and RA Kowluru. (2008). Oxidative stress and diabetic retinopathy: pathophysiological mechanisms and treatment perspectives. Rev Endocr Metab Disord 9:315–327.
13. Huang Y, V Enzmann and ST Ildstad. (2011). Stem cell-based therapeutic applications in retinal degenerative diseases. Stem Cell Rev 7:434–445.
14. Davey GC, SB Patil, A O'Loughlin and T O'Brien. (2014). Mesenchymal stem cell-based treatment for microvascular and secondary complications of diabetes mellitus. Front Endocrinol (Lausanne) 5:86.
15. Traktuev DO, S Merfeld-Clauss, J Li, M Kolonin, W Arap, R Pasqualini, BH Johnstone and KL March. (2008). A population of multipotent CD34-positive adipose stromal cells share pericyte and mesenchymal surface markers, reside in a periendothelial location, and stabilize endothelial networks. Circ Res 102:77–85.
16. Merfeld-Clauss S, N Gollahalli, KL March and DO Traktuev. (2010). Adipose tissue progenitor cells directly interact with endothelial cells to induce vascular network formation. Tissue Eng Part A 16:2953–2966.
17. Rajashekhar G, A Ramadan, C Abburi, B Callaghan, DO Traktuev, C Evans-Molina, R Maturi, A Harris, TS Kern and KL March. (2014). Regenerative therapeutic potential of adipose stromal cells in early stage diabetic retinopathy. PLoS One 9:e84671.
18. Mendel TA, EB Clabough, DS Kao, TN Demidova-Rice, JT Durham, BC Zotter, SA Seaman, SM Cronk, EP Rakoczy, et al. (2013). Pericytes derived from adipose-derived stem cells protect against retinal vasculopathy. PLoS One 8:e65691.
19. Bourin P, BA Bunnell, L Casteilla, M Dominici, AJ Katz, KL March, H Redl, JP Rubin, K Yoshimura and JM Gimble. (2013). Stromal cells from the adipose tissue-derived stromal vascular fraction and culture expanded adipose tissue-derived stromal/stem cells: a joint statement of the International Federation for Adipose Therapeutics and Science (IFATS) and the International Society for Cellular Therapy (ISCT). Cytotherapy 15:641–648.
20. Burgess WH, T Mehlman, R Friesel, WV Johnson and T Maciag. (1985). Multiple forms of endothelial cell growth factor. Rapid isolation and biological and chemical characterization. J Biol Chem 260:11389–11392.
21. Eruslanov E and S Kusmartsev. (2010). Identification of ROS using oxidized DCFDA and flow-cytometry. Methods Mol Biol 594:57–72.
22. Trudeau K, AJ Molina and S Roy. (2011). High glucose induces mitochondrial morphology and metabolic changes in retinal pericytes. Invest Ophthalmol Vis Sci 52:8657–8664.

23. Lu Y, SG Rolland and B Conradt. (2011). A molecular switch that governs mitochondrial fusion and fission mediated by the BCL2-like protein CED-9 of Caenorhabditis elegans. Proc Natl Acad Sci U S A 108:E813–E822.
24. Regmi SG, SG Rolland and B Conradt. (2014). Age-dependent changes in mitochondrial morphology and volume are not predictors of lifespan. Aging (Albany NY) 6: 118–130.
25. Gariano RF. (2010). Special features of human retinal angiogenesis. Eye (Lond) 24:401–407.
26. Calcutt NA, ME Cooper, TS Kern and AM Schmidt. (2009). Therapies for hyperglycaemia-induced diabetic complications: from animal models to clinical trials. Nat Rev Drug Discov 8:417–429.
27. Trudeau K, AJ Molina, W Guo and S Roy. (2010). High glucose disrupts mitochondrial morphology in retinal endothelial cells: implications for diabetic retinopathy. Am J Pathol 177:447–455.
28. Kroemer G. (1997). Mitochondrial implication in apoptosis. Towards an endosymbiont hypothesis of apoptosis evolution. Cell Death Differ 4:443–456.
29. Xie L, X Zhu, Y Hu, T Li, Y Gao, Y Shi and S Tang. (2008). Mitochondrial DNA oxidative damage triggering mitochondrial dysfunction and apoptosis in high glucose-induced HRECs. Invest Ophthalmol Vis Sci 49:4203–4209.
30. Rego AC and CR Oliveira. (2003). Mitochondrial dysfunction and reactive oxygen species in excitotoxicity and apoptosis: implications for the pathogenesis of neurodegenerative diseases. Neurochem Res 28:1563–1574.
31. Kowluru RA. (2005). Diabetic retinopathy: mitochondrial dysfunction and retinal capillary cell death. Antioxid Redox Signal 7:1581–1587.
32. Karbowski M and RJ Youle. (2003). Dynamics of mitochondrial morphology in healthy cells and during apoptosis. Cell Death Differ 10:870–880.
33. Scorrano L. (2007). Multiple functions of mitochondria-shaping proteins. Novartis Found Symp 287:47–55; discussion 55–59.

Address correspondence to:
Prof. Martin C. Harmsen
Department of Pathology and Medical Biology
University Medical Center Groningen
University of Groningen
Hanzeplein 1(EA11)
Groningen 9713 GZ
The Netherlands

E-mail: m.c.harmsen@umcg.nl

Received for publication January 26, 2016
Accepted after revision July 29, 2016
Prepublished on Liebert Instant Online July 29, 2016